

# Pulse-Bandwidth Dependence of Coherent Phase Control of Resonance-Mediated (2+1) Three-Photon Absorption

Andrey Gandman, Lev Chuntunov, Leonid Rybak, and Zohar Amitay\*

*Schulich Faculty of Chemistry, Technion - Israel Institute of Technology, Haifa 32000, Israel*

## Abstract

We study in detail coherent phase control of femtosecond resonance-mediated (2+1) three-photon absorption and its dependence on the spectral bandwidth of the excitation pulse. The regime is the weak-field regime of third perturbative order. The corresponding interference mechanism involves a group of three-photon excitation pathways that are on resonance with the intermediate state and a group of three-photon excitation pathways that are near resonant with it. The model system of the study is atomic sodium (Na), for which experimental and numerical-theoretical results are obtained. Prominent among the results is our finding that with simple proper pulse shaping an increase in the excitation bandwidth leads to a corresponding increase in the enhancement of the three-photon absorption over the absorption induced by the (unshaped) transform-limited pulse. For example, here, a 40-nm bandwidth leads to an order-of-magnitude enhancement over the transform-limited absorption.

PACS numbers: 32.80.Qk, 32.80.Wr, 42.65.Re

---

\*Electronic address: amitayz@tx.technion.ac.il

## I. INTRODUCTION

Coherent control utilizes the coherent nature of the light in order to control transition probabilities of the irradiated quantum system to desired target states [1, 2, 3, 4, 5]. Due to their broad spectrum, femtosecond pulses provide a wide coherent band of such photo-induced pathways. The control is achieved by manipulating interferences among multiple initial-to-final state-to-state pathways. Constructive interferences enhance the transition probability, while destructive interferences attenuate it. The interferences are manipulated by shaping the pulse, i.e., manipulating the phase, amplitude, and/or polarization of its various spectral components.

Prominent among the processes, over which such femtosecond control has been demonstrated to be very effective, are multiphoton processes that are of fundamental as well as applicative importance for nonlinear spectroscopy and microscopy [5, 6, 7, 8, 9, 10, 11, 12, 13, 14, 15, 16, 17, 18, 19, 20, 21]. For a given energy, manipulating the pulse shape manipulates the cross-section of the corresponding process. For rational shaping of femtosecond pulses, which are favorable for a desired result, the most convenient excitation regime is the weak-field regime where the photo-excitation is validly described within the time-dependent perturbation theory of the lowest non-vanishing order. For N-photon absorption processes it is the  $N^{th}$  order. Such a description allows a transformation of the photo-excitation picture into the frequency domain, where the interfering pathways and their interference mechanism can be identified and serve as a basis for the rational pulse shaping. Corresponding examples of past control studies include the control over non-resonant two-photon absorption [6, 7] and resonance-mediated (1+1) two-photon absorption [8, 9, 10] in atoms, over non-resonant two-photon absorption and non-resonant three-photon absorption in large molecules [11], over molecular Raman transitions [12], and over molecular coherent anti-Stokes Raman scattering (CARS) [13, 14].

In addition to these multiphoton control works, in a recent study we firstly analyzed theoretically and demonstrated experimentally coherent phase control over the process of atomic resonance-mediated (2+1) three-photon absorption [15]. The present work is a direct continuation of this first work. It extends the analysis of the corresponding interference mechanism and obtains new physical insight regarding its dependence on the spectral bandwidth of the excitation pulse. The model system of the study is atomic sodium (Na).

Section II of the paper gives the corresponding frequency-domain theoretical description of the process as obtained based on  $3^{rd}$ -order time-dependent perturbation theory. The paper ends with conclusions in Sec. V. Section III A describes the Na model system and the families of shaped pulses that serve as test cases. It follows by Sec. III B that presents corresponding experimental results that re-confirm the theoretical description and corresponding numerical calculations. Then, Sec. III C presents extended numerical-theoretical results that fully reveal the spectral-bandwidth dependence of the process, as discussed in Sec. IV.

## II. FREQUENCY-DOMAIN THEORETICAL DESCRIPTION

As shown in Fig. 1, the resonance-mediated (2+1) three-photon absorption process considered here involves an initial state  $|g\rangle$ , a final state  $|f\rangle$ , and an intermediate state  $|r\rangle$ . The  $|g\rangle$  and  $|r\rangle$  states are coupled by a non-resonant two-photon coupling provided by a manifold of states  $|v\rangle$  that are far from resonance, i.e., half the two-photon transition frequency  $\omega_{rg}/2$  falls within the pulse spectrum while the  $|g\rangle$ - $|v\rangle$  transition frequencies  $\omega_{vg}$  fall outside the pulse spectrum. The  $|f\rangle$ - $|r\rangle$  coupling is a resonant one-photon coupling, i.e., the corresponding transition frequency  $\omega_{fr}$  falls within the pulse spectrum.

In a weak-field regime the three-photon absorption is validly described by third-order time-dependent perturbation theory. Accordingly, the time-dependent (complex) amplitude  $a_f(t)$  of state  $|f\rangle$  at time  $t$ , due to the interaction with the shaped temporal electric field  $\varepsilon(t)$ , is given by

$$a_f(t) = -\frac{1}{i\hbar^3} \sum_v \mu_{fr} \mu_{rv} \mu_{vg} \int_{-\infty}^t \int_{-\infty}^{t_1} \int_{-\infty}^{t_2} \varepsilon(t_1) \varepsilon(t_2) \varepsilon(t_3) \times \exp(i\omega_{fr}t_1) \exp(i\omega_{rv}t_2) \exp(i\omega_{vg}t_3) dt_1 dt_2 dt_3, \quad (1)$$

where  $\mu_{mn} = \langle m | \mu | n \rangle$  and  $\omega_{mn} = (E_m - E_n)/\hbar$  are, respectively, the dipole matrix element and the transition frequency between a pair of states  $|m\rangle$  and  $|n\rangle$ . The transition frequencies  $\omega_{rg}$ ,  $\omega_{fr}$ , and  $\omega_{fg}$  satisfy the relation  $\omega_{fg} = \omega_{fr} + \omega_{rg}$ .

Within the frequency-domain framework, the spectral field of the pulse  $E(\omega) \equiv |E(\omega)| \exp[i\Phi(\omega)]$  is given as the Fourier transform of  $\varepsilon(t)$ , with  $|E(\omega)|$  and  $\Phi(\omega)$  being, respectively, the spectral amplitude and phase of frequency  $\omega$ . For the unshaped transform-limited (TL) pulse,  $\Phi(\omega) = 0$  for any  $\omega$ . We also define the normalized spectral field  $\tilde{E}(\omega) \equiv E(\omega)/|E_0| \equiv \left| \tilde{E}(\omega) \right| \exp[i\Phi(\omega)]$  that represents the pulse shape, where  $|E_0|$  is the

peak spectral amplitude. This allows to clearly distinguish in the expressions given below between the dependence on the pulse intensity and the dependence on the pulse shape. The maximal spectral intensity  $I_0$  is proportional to  $|E_0|^2$  ( $I_0 \propto |E_0|^2$ ). The resonance-mediated (2+1) three-photon excitation scheme implies that  $|\tilde{E}(\omega_{rg}/2)| \neq 0$ ,  $|\tilde{E}(\omega_{vg})| = 0$ , and  $|\tilde{E}(\omega_{fr})| \neq 0$ . Then, the final amplitude  $A_f^{(2+1)} \equiv a_f(t \rightarrow \infty)$  of state  $|f\rangle$  after the pulse is over ( $t \rightarrow \infty$ ) is obtained to be [15]

$$A_f^{(2+1)} = \frac{1}{\hbar^3} \mu_{fr} \mu_{rg}^2 |E_0|^3 \left[ A_f^{(2+1)on-res} + A_f^{(2+1)near-res} \right], \quad (2)$$

where  $\mu_{fr}$  is the  $|f\rangle$ - $|r\rangle$  dipole matrix element and  $\mu_{rg}^2$  is the  $|r\rangle$ - $|g\rangle$  effective non-resonant two-photon dipole coupling [6]. The terms  $A_f^{(2+1)on-res}$  and  $A_f^{(2+1)near-res}$  are given by

$$A_f^{(2+1)on-res} = i\pi \tilde{E}(\omega_{fr}) A^{(2)}(\omega_{rg}), \quad (3)$$

$$A_f^{(2+1)near-res} = -\wp \int_{-\infty}^{\infty} \frac{1}{\delta} A^{(2)}(\omega_{rg} - \delta) \tilde{E}(\omega_{fr} + \delta) d\delta, \quad (4)$$

with

$$A^{(2)}(\Omega) = \int_{-\infty}^{\infty} \tilde{E}(\omega) \tilde{E}(\Omega - \omega) d\omega. \quad (5)$$

The expressions of Eqs. (2)-(5) are equivalent to the ones given in Ref. [15]. However, as shown below, they are given here in a different form that provides deeper and more intuitive physical insight to the femtosecond excitation process.

The final amplitude  $A_f^{(2+1)}$  of  $|f\rangle$  coherently interferes all the possible three-photon pathways from  $|g\rangle$  to  $|f\rangle$ , i.e., coherently integrates over all their corresponding amplitudes. Several pathway examples are shown schematically in Fig. 1. Each three-photon pathway is either on-resonance or near-resonance with the intermediate state  $|r\rangle$ , with a corresponding detuning  $\delta$ . A resonance-mediated (2+1) three-photon pathway corresponding to a detuning  $\delta$  involves a non-resonant absorption of two photons to a total excitation energy of  $\omega_{rg} - \delta$  and the absorption of a third photon of frequency  $\omega_{fr} + \delta$ . The term  $A_f^{(2+1)on-res}$  interferes all the on-resonant pathways ( $\delta = 0$ ), while the term  $A_f^{(2+1)near-res}$  interferes all the near-resonant pathways ( $\delta \neq 0$ ) with an amplitude weighting of  $1/\delta$  (i.e., inversely proportional to its detuning). The on-resonant pathways are excluded from  $A_f^{(2+1)near-res}$  by the Cauchy's principal value operator  $\wp$ . Thus, the resulting absorption is determined by both intra-group and inter-group interferences involving these two groups of three-photon excitation pathways. Both  $A_f^{(2+1)on-res}$  and  $A_f^{(2+1)near-res}$  terms are expressed using the term

$A^{(2)}(\Omega)$  that is proportional to the non-resonant two-photon absorption amplitude to a total transition frequency of  $\Omega$ . It interferes all the corresponding two-photon pathways. The phase associated with each two-photon pathway is equal to the sum of the phases of the two corresponding photons. So, with the transform-limited (TL) pulse all the two-photon pathways acquire zero phase for any value of  $\Omega$  and, thus, interfere one with the other in a fully constructive way. For a given field spectrum  $|\tilde{E}(\omega)|$ , this leads to the maximal  $A^{(2)}(\Omega)$  for any value of  $\Omega$ . For a given  $\Omega$ , any spectral phase pattern that is anti-symmetric around  $\Omega/2$  also induces fully constructive interferences among all the two-photon pathways of  $\Omega$  transition frequency, and thus it induces the corresponding maximal  $A^{(2)}(\Omega)$  as the TL pulse. As can be seen from Eq. (5),  $A^{(2)}(\Omega)$  is actually the (complex) convolution function of the (complex) field  $\tilde{E}(\omega)$  evaluated at  $\Omega$ . Since  $A_f^{(2+1)on-res}$  is proportional to  $A^{(2)}(\omega_{rg})$ , it is actually proportional to the weak-field non-resonant two-photon absorption amplitude to  $|r\rangle$ , as obtained by second-order perturbation theory [6].

The final population  $P_f^{(2+1)}$  of state  $|f\rangle$ , given by  $P_f^{(2+1)} = |A_f^{(2+1)}|^2$ , serves as the measure for the resonance-mediated (2+1) three-photon absorption. All the results presented here are given relative to the absorption induced by the transform-limited (TL) pulse. So, for convenience, we introduce the TL-normalized three-photon absorption measure  $\tilde{P}_f^{(2+1)} = P_f^{(2+1)}/P_{f,TL}^{(2+1)}$ , where  $P_{f,TL}^{(2+1)}$  is the final  $|f\rangle$  population induced by the TL pulse.

### III. RESULTS

#### A. Model system and pulse-shape test cases

The model system of the study is the sodium (Na) atom [23], with the corresponding excitation scheme shown in Fig. 1. It involves the  $3s$  ground state as  $|g\rangle$ , the  $4s$  state as  $|r\rangle$ , and the  $7p$  state as  $|f\rangle$ . The transition frequency  $\omega_{rg} \equiv \omega_{4s,3s} = 25740 \text{ cm}^{-1}$  corresponds to two 777 nm photons and the transition frequency  $\omega_{fr} \equiv \omega_{7p,4s} = 12801 \text{ cm}^{-1}$  corresponds to a one 781.2 nm photon. The  $3s$ - $4s$  non-resonant two-photon coupling originates from the manifold of  $p$ -states, particularly from the  $3p$  state [ $\omega_{3p,3s} \sim 16978 \text{ cm}^{-1}$  (589 nm)]. The absorption measure is the final  $7p$  population  $P_f^{(2+1)} \equiv P_{7p}^{(2+1)}$ .

As the test cases for coherent phase control, the present study uses shaped femtosecond pulses having two sets of spectral phase patterns,  $\Phi^{(\text{SNstep})}(\omega)$  and  $\Phi^{(\text{DBstep})}(\omega)$ . They are

shown schematically in the inset of Fig. 1. The  $\Phi^{(\text{SNstep})}(\omega)$  set includes the phase patterns of a single  $\pi$  step, each characterized by the  $\pi$  step position  $\omega_{\text{step}}^{(\text{SNstep})}$ . The  $\Phi^{(\text{DBstep})}(\omega)$  set includes the phase patterns composed of two  $\pi$  steps, with the two steps located at equal distance along the frequency axis from both sides (i.e., to the blue and to the red) of half the two-photon transition frequency  $\omega_{4s,3s}/2$ , i.e.,  $\omega_{4s,3s}/2 - \omega_{\text{left-step}}^{(\text{DBstep})} = \omega_{\text{right-step}}^{(\text{DBstep})} - \omega_{4s,3s}/2 \equiv \Delta_{\text{step}}^{(\text{DBstep})}$ . In our previous work [15] the single-step phase patterns have been shown to be very effective in controlling the resonance-mediated (2+1) three-photon absorption. The double-step phase patterns are additionally included here since, as explained below, they all induce the same maximal on-resonant component  $A_{7p}^{(2+1)\text{on-res}}$ , while each of them induces a different near-resonant component  $A_{7p}^{(2+1)\text{near-res}}$ .

The  $\pi$  amplitude of all the phase steps, i.e., generally  $\Phi(\omega) = 0$  or  $\pi$ , implies that the field  $\tilde{E}(\omega)$  is always a real (positive or negative) quantity for any  $\omega$ . Thus, the corresponding  $A_{7p}^{(2+1)\text{on-res}}$  and  $A_{7p}^{(2+1)\text{near-res}}$  are, respectively, purely imaginary and real [see Eqs. (3)-(4)], and  $P_{7p}^{(2+1)} \propto \left| A_{7p}^{(2+1)\text{on-res}} \right|^2 + \left| A_{7p}^{(2+1)\text{near-res}} \right|^2$ . Consequently,  $\tilde{P}_{7p}^{(2+1)} = \left| \tilde{A}_{7p}^{(2+1)\text{on-res}} \right|^2 + \left| \tilde{A}_{7p}^{(2+1)\text{near-res}} \right|^2$ , where  $\left| \tilde{A}_{7p}^{(2+1)\text{on-res}} \right|^2 = \left| A_{7p}^{(2+1)\text{on-res}} \right|^2 / P_{7p,\text{TL}}^{(2+1)}$  and  $\left| \tilde{A}_{7p}^{(2+1)\text{near-res}} \right|^2 = \left| A_{7p}^{(2+1)\text{near-res}} \right|^2 / P_{7p,\text{TL}}^{(2+1)}$ . In other words, with the spectral phase patterns discussed here, the absorption is determined only by intra-group interferences taking place separately within each of the on-resonant and near-resonant excitation groups, without any inter-group interferences taking place. This fact greatly simplifies, without reduction of generality, the ability to gain physical insight into the pulse-bandwidth dependence of the resonance-mediated (2+1) three-photon absorption process.

## B. Experimental vs. numerical-theoretical results

This section presents experimental results for the Na atom, re-confirming the above theoretical description with spectral parameters, i.e., spectral bandwidth and the above phase patterns, that are different from those used in our previous work [15]. Experimentally, atomic sodium vapor is produced in a static chamber at 300°C (Na partial pressure of  $\sim 0.1$  Torr) with 10-Torr Ar buffer gas. It is irradiated at a 1-kHz repetition rate with linearly-polarized shaped femtosecond laser pulses of 9.8-nm ( $160\text{-cm}^{-1}$ ) intensity bandwidth (FWHM) around 781 nm ( $12804\text{ cm}^{-1}$ ). The spectrum shape is a modified Gaussian with a slight asymmetry toward low frequencies. It is shown in the inset of Fig. 2(a1). Experiments are also con-

ducted with a spectrum that results from blocking about half of this full spectrum at a cutoff wavelength of 783 nm ( $12771 \text{ cm}^{-1}$ ). It is shown in the inset of Fig. 2(b1). In both spectral cases, the temporal peak intensity of the corresponding transform-limited (TL) pulse is below  $10^9 \text{ W/cm}^2$ . The laser pulses undergo shaping in a  $4f$  optical setup incorporating a pixelated liquid-crystal spatial light phase modulator [22]. The effective spectral shaping resolution is  $\delta\omega_{shaping} = 2.05 \text{ cm}^{-1}$  (0.125 nm) per pixel. Following the interaction with a pulse, the Na population excited to the  $7p$  state undergoes radiative and collisional decay to lower excited states, including the  $4d$ ,  $5d$ ,  $6d$ , and  $6s$  states. The fluorescence emitted in their decay to the  $3p$  state serves as the relative measure for the total final  $7p$  population  $P_{7p}^{(2+1)}$ . It is optically measured at  $90^\circ$  to the beam propagation direction using a spectrometer coupled to a time-gated camera system.

Figure 2 compares the experimental results (circles or squares) with corresponding theoretical results (solid lines) for the resonance-mediated (2+1) three-photon absorption in Na. The theoretical results are calculated numerically using Eqs. (2)-(5), using a grid with a bin size equal to the experimental spectral shaping resolution  $\delta\omega_{shaping}$ . Figures 2(a1) and 2(a2) (first-row panels) correspond to the full pulse spectrum [inset of Fig. 2(a1)], while Figs. 2(b1) and 2(b2) (second-row panels) correspond to the blocked pulse spectrum [inset of Fig. 2(b1)]. Figures 2(a1) and 2(b1) (left-column panels) present results for the single-step set of spectral phase patterns  $\Phi^{(\text{SNstep})}(\omega)$ . The corresponding traces show the TL-normalized final  $7p$  population  $\tilde{P}_{7p}^{(2+1)}$  (see above) as a function of the single  $\pi$ -step position  $\omega_{\text{step}}^{(\text{SNstep})}$ . Figures 2(a2) and 2(b2) (right-column panels) present results for the double-step set of spectral phase patterns  $\Phi^{(\text{DBstep})}(\omega)$ . The corresponding traces show the TL-normalized final  $7p$  population  $\tilde{P}_{7p}^{(2+1)}$  (see above) as a function of the left  $\pi$ -step position  $\omega_{\text{left-step}}^{(\text{DBstep})}$ .

As can be seen, there is an excellent quantitative agreement between the experimental results ("real experiment") and the numerical-theoretical results ("computer experiment"). Hence, supported also by our previous work [15], the validity and accuracy of the theoretical description and numerical calculations are re-confirmed. As such, in the following they serve us for the detailed study of the  $\pi$ -traces, their spectral-bandwidth dependence, and the corresponding interference mechanism.

### C. Numerical-theoretical results

Figure 3 presents theoretical results (solid lines) that have been calculated numerically for the resonance-mediated (2+1) three-photon absorption in Na with excitation pulse of different spectral bandwidth. In all the cases the intensity spectrum is a Gaussian centered at 780 nm (12821 cm<sup>-1</sup>). The corresponding bandwidth (FWHM) values ( $\Delta\omega$ ) are (a) 5 nm (82 cm<sup>-1</sup>), (b) 9 nm (148 cm<sup>-1</sup>), (c) 15 nm (247 cm<sup>-1</sup>), (d) 25 nm (411 cm<sup>-1</sup>), and (e) 40 nm (658 cm<sup>-1</sup>). Each row in the figure corresponds to a different bandwidth. As indicated above, the numerical calculations are based on Eqs. (2)-(5) and use a grid with a bin size equal to the experimental spectral shaping resolution.

The left-column panels of Fig. 3 correspond to the single-step spectral phase patterns  $\Phi^{(\text{SNstep})}(\omega)$ . In solid lines they show the TL-normalized final  $7p$  population  $\tilde{P}_{7p}^{(2+1)}$  as a function of the single  $\pi$ -step position  $\omega_{\text{step}}^{(\text{SNstep})}$ . Additionally, they also show the corresponding on-resonant component  $\left|\tilde{A}_{7p}^{(2+1)\text{on-res}}\right|^2$  (dotted lines) and the near-resonant component  $\left|\tilde{A}_{7p}^{(2+1)\text{near-res}}\right|^2$  (dashed lines), satisfying  $\tilde{P}_{7p}^{(2+1)} = \left|\tilde{A}_{7p}^{(2+1)\text{on-res}}\right|^2 + \left|\tilde{A}_{7p}^{(2+1)\text{near-res}}\right|^2$  (see above). As can be seen, the shape of the traces strongly depends on the spectral bandwidth. For any given bandwidth, the three-photon absorption is tunable over a wide range of values, from a low attenuated level below 0.01 of the TL absorption to a high enhanced level with a value that strongly depends on the spectral bandwidth. Whenever this enhanced absorption exceeds the TL absorption, it occurs when  $\omega_{\text{step}}^{(\text{SNstep})} = \omega_{7p,4s}$ , i.e., when the  $\pi$ -step is located at the  $7p$ - $4s$  transition frequency. This is actually the location of the prominent feature of the single-step traces. As seen in Fig. 3, as the spectral bandwidth increases from 5 nm to 9 nm to 15 nm, the value of  $\tilde{P}_{7p}^{(2+1)}$  at  $\omega_{\text{step}}^{(\text{SNstep})} = \omega_{7p,4s}$  decreases, respectively, from 2.5 to 1.1 to below 0.01. Then, further increase in the bandwidth leads to its increase to a value of 1.4 at 25-nm bandwidth and to a value of 4.1 at 40-nm bandwidth. Another prominent bandwidth dependence is observed for the TL pulse regarding the relative weight of the corresponding on-resonant and near-resonant amplitude components, as it is reflected in the asymptotes of the single-step traces: As the bandwidth increases, the TL on-resonant component dominates more and more the total absorption, approaching the limit of  $\left|A_{7p,\text{TL}}^{(2+1)\text{near-res}}\right| \ll \left|A_{7p,\text{TL}}^{(2+1)\text{on-res}}\right|$  and  $\left|\tilde{A}_{7p,\text{TL}}^{(2+1)\text{on-res}}\right|^2 \rightarrow 1$ .

The right-column panels of Fig. 3 correspond to the double-step spectral phase patterns  $\Phi^{(\text{DBstep})}(\omega)$ . They show the TL-normalized final  $7p$  population  $\tilde{P}_{7p}^{(2+1)}$  as a function of the left



$\pi$ -step position  $\omega_{\text{left-step}}^{(\text{DBstep})}$ . One should note that the maximal value of the y-axis in these traces is higher than in the traces of the single-step phase patterns (the left-column panels). The prominent feature of the double-step traces is the strong absorption enhancement occurring when  $\omega_{\text{left-step}}^{(\text{DBstep})} = \omega_{7p,4s}$ . This is also the step-position region, where the dependence on the spectral bandwidth is the strongest. The corresponding enhancement value is always above one, i.e., above the TL absorption, and it continuously increases as the bandwidth increases. It starts from a value of 2.8 at 5-nm bandwidth [Fig. 3(a2)] and reaches a value of 7.2 at 40-nm bandwidth [Fig. 3(e2)]. When  $\omega_{\text{left-step}}^{(\text{DBstep})}$  is far from  $\omega_{7p,4s}$ , the three-photon absorption is always kept on a level that is very close to or equal to the TL absorption. The only exception is the case of 5-nm bandwidth [Fig. 3(a2)], where at step positions higher than  $\omega_{7p,4s}$  the absorption is reduced to a level of about half the TL absorption.

As can be seen in Fig. 3, the main features of the traces when  $\omega_{\text{step}}^{(\text{SNstep})} = \omega_{7p,4s}$  and when  $\omega_{\text{left-step}}^{(\text{DBstep})} = \omega_{7p,4s}$  originate from the near-resonant component  $\left| \tilde{A}_{7p}^{(2+1)\text{near-res}} \right|^2$ . Thus, to complete the picture, Fig. 4 presents extended results for the spectral-bandwidth dependence of the resonance-mediated (2+1) three-photon absorption when  $\omega_{\text{step}}^{(\text{SNstep})} = \omega_{7p,4s}$  in a single-step pattern [Fig. 4(a)] and when  $\omega_{\text{left-step}}^{(\text{DBstep})} = \omega_{7p,4s}$  in a double-step pattern [Fig. 4(b)]. The figure presents the corresponding values of  $\tilde{P}_f^{(2+1)}$  (solid lines),  $\left| \tilde{A}_{7p}^{(2+1)\text{on-res}} \right|^2$  (dotted lines), and  $\left| \tilde{A}_{7p}^{(2+1)\text{near-res}} \right|^2$  (dashed lines) as a function of the spectral bandwidth. The bandwidth values span the wide range of 2 to 40 nm that corresponds, respectively, to a TL pulse duration of 450 down to 22 fs. As can be seen, with the single-step phase pattern of  $\omega_{\text{step}}^{(\text{SNstep})} = \omega_{7p,4s}$ , the degree of absorption is between 0.01 to 4 times the TL absorption, i.e., it is either enhanced or attenuated as compared to the TL case. There is a local peak of value 2.55 at a bandwidth of 5.25 nm, and a minimum of zero theoretical value (i.e., three-photon dark pulse) at a bandwidth value of 14.6 nm. Then, above 14.6 nm,  $\tilde{P}_f^{(2+1)}$  is monotonically increases with the increase in the bandwidth. At 23-nm bandwidth it reaches a value of 1, at 32 nm it reaches again a value of 2.5, and at 40 nm it reaches a value of 4.1. On the other hand, with the double-step phase pattern of  $\omega_{\text{left-step}}^{(\text{DBstep})} = \omega_{7p,4s}$ , the absorption is always above the TL absorption and the corresponding enhancement monotonically increases with the increase in the spectral bandwidth. At 2-nm bandwidth  $\tilde{P}_{7p}^{(2+1)}$  is of a value of 1, and it reaches a value of 7.2 at a bandwidth of 40 nm. As can be seen in Fig. 4, in both these single-step and double-step patterns having the step at  $\omega_{7p,4s}$ , over the full bandwidth range, the

near-resonant component  $\left| \tilde{A}_{7p}^{(2+1)near-res} \right|^2$  is much larger than the on-resonant component  $\left| \tilde{A}_{7p}^{(2+1)on-res} \right|^2$ .

#### IV. ANALYSIS AND DISCUSSION

Below, the main features of the results presented above are analyzed based on the theoretical description formulated in Eqs. (2)-(5). As noted above, for the spectral phase patterns used here, the resonance-mediated (2+1) three-photon absorption is determined only by intra-group interferences within each of the on-resonant and near-resonant excitation groups that correspond, respectively, to  $A_{7p}^{(2+1)on-res}$  and  $A_{7p}^{(2+1)near-res}$ , with the relations  $P_{7p}^{(2+1)} \propto \left| A_{7p}^{(2+1)on-res} \right|^2 + \left| A_{7p}^{(2+1)near-res} \right|^2$  and  $\tilde{P}_{7p}^{(2+1)} = \left| \tilde{A}_{7p}^{(2+1)on-res} \right|^2 + \left| \tilde{A}_{7p}^{(2+1)near-res} \right|^2$ .

The analysis uses the numerical results presented in Fig. 5. Each panel in the figure corresponds to a pulse having a different spectral bandwidth for its Gaussian intensity spectrum around 780 nm. The corresponding bandwidth values are (a) 5 nm, (b) 9 nm, (c) 15 nm, (d) 25 nm, and (e) 40 nm, as they are in the results shown in Fig. 3. Each panel shows results for the transform-limited (TL) pulse (dashed black line), for the shaped pulse with the single-step phase pattern of  $\omega_{step}^{(SNstep)} = \omega_{7p,4s}$  (solid gray line), and for the shaped pulse with the double-step phase pattern of  $\omega_{left-step}^{(DBstep)} = \omega_{7p,4s}$  (solid black line). For the different cases, the values of  $A^{(2)}(\Omega = \omega_{4s,3s} - \delta)$  [see Eq. (5)] are shown as a function of the detuning  $\delta$  from the 4s state. The detuning (x-axis) values are actually given as normalized values of  $\delta/\Delta\omega$ , with  $\Delta\omega$  being the bandwidth of the intensity spectrum.

As seen from Eq. (3), the value of the on-resonant component  $A_{7p}^{(2+1)on-res}$  is proportional to  $A^{(2+1)}(0) \equiv A^{(2)}(\omega_{4s,3s})\tilde{E}(\omega_{7p,4s})$  that corresponds to zero detuning  $\delta = 0$ . On the other hand, as seen from Eq. (4), due to the  $1/\delta$ -weighting, the result of the  $\varphi$ -integration of  $A_{7p}^{(2+1)near-res}$  is dominated by the integration over small non-zero values of  $|\delta|$  around  $\delta=0$ . Due to the sign change of  $1/\delta$  for  $\pm|\delta|$ , the  $\varphi$ -integration result is highly sensitive to the symmetry of the integrand term  $A^{(2+1)}(\delta) \equiv A^{(2)}(\omega_{4s,3s} - \delta)\tilde{E}(\omega_{7p,4s} + \delta)$  around  $\delta=0$ , i.e., its relative magnitude and relative sign for positive and negative detunings of equal magnitude (i.e.,  $\pm|\delta|$ ). The zone of small  $|\delta|$  around  $\delta=0$  is indicated schematically as dashed area in Fig. 5.

### A. Transform-limited pulse

First we analyze the case of the transform-limited (TL) pulse (dashed thin black lines in Fig. 5). Since  $A^{(2)}(\Omega)$  is the convolution function of  $\tilde{E}(\omega)$  evaluated at  $\Omega$ , for the TL pulse [ $\Phi(\omega) = 0$ ] it is actually a convolution of  $\left| \tilde{E}(\omega) \right|$  with a real positive values for any  $\Omega$ . Thus, with a Gaussian spectrum around  $\omega_0$ ,  $A_{\text{TL}}^{(2)}(\Omega)$  has a Gaussian shape that is peaked at  $\Omega_{\text{peak}} = 2\omega_0$ . The corresponding detuning is  $\delta_{\text{peak}} = \omega_{4s,3s} - 2\omega_0$ . The width (FWHM) of the  $A_{\text{TL}}^{(2)}(\Omega)$  Gaussian profile is  $2\Delta\omega$ , where  $\Delta\omega$  is the width of the intensity spectrum. Since the detuning values given in Fig. 5 are normalized by  $\Delta\omega$ , all the presented TL profiles of  $A_{\text{TL}}^{(2)}(\Omega = \omega_{4s,3s} - \delta)$  have the same width (of value 2) for any spectral bandwidth  $\Delta\omega$ . On the other hand, an increase in  $\Delta\omega$  leads to a decrease in the value of  $\delta_{\text{peak}}/\Delta\omega$ . Hence, as seen in Fig. 5, as  $\Delta\omega$  increases, the peak and the full profile of  $A_{\text{TL}}^{(2)}(\omega_{4s,3s} - \delta)$  shifts to smaller values of  $\delta/\Delta\omega$  and the corresponding value of  $A_{\text{TL}}^{(2)}(\omega_{4s,3s})$ , which determines the on-resonant component  $A_{7p,\text{TL}}^{(2+1)\text{on-res}}$ , increases.

For the TL pulse, both  $A_{\text{TL}}^{(2)}(\omega_{4s,3s} - \delta)$  and  $\tilde{E}_{\text{TL}}(\omega_{7p,4s} + \delta)$  are real positive quantities for any  $\delta$ . Thus, since the sign of  $1/\delta$  is different for  $+\delta$  and  $-\delta$ , the amplitudes  $\frac{1}{\delta}A_{\text{TL}}^{(2+1)}(\delta)$  contributed by  $\pm|\delta|$  to the  $\wp$ -integration of  $A_{7p,\text{TL}}^{(2+1)\text{near-res}}$  are of different signs, i.e., they interfere destructively one with the other.

As a result from all the above, an increase of  $\Delta\omega$  leads to a decrease in the value of  $\left| \frac{1}{|\delta|}A_{\text{TL}}^{(2+1)}(+|\delta|) - \frac{1}{|\delta|}A_{\text{TL}}^{(2+1)}(-|\delta|) \right| / \left| A_{\text{TL}}^{(2+1)}(0) \right|$  for a given small  $|\delta|$ . Consequently, there is a decrease in the relative magnitude between the TL near-resonant component  $A_{7p,\text{TL}}^{(2+1)\text{near-res}}$  and the TL on-resonant component  $A_{7p,\text{TL}}^{(2+1)\text{on-res}}$ . Eventually, at large enough  $\Delta\omega$ , it leads to  $\left| A_{7p,\text{TL}}^{(2+1)\text{near-res}} \right| \ll \left| A_{7p,\text{TL}}^{(2+1)\text{on-res}} \right|$ ,  $P_{7p,\text{TL}}^{(2+1)} \rightarrow \left| A_{7p,\text{TL}}^{(2+1)\text{on-res}} \right|^2$ , and  $\left| \tilde{A}_{7p,\text{TL}}^{(2+1)\text{on-res}} \right|^2 \rightarrow 1$ . As noted above, this is indeed the behavior seen in the asymptotes of the single-step traces shown in the left-column panels of Fig. 3 (dashed and dotted lines). In other words, for the TL pulse, with large enough bandwidth, the absorption amplitudes contributed by positively-detuned and negatively-detuned near-resonant three-photon pathways completely cancel out each other. Then, the total TL absorption is determined only by the three-photon pathways that are on-resonant with the intermediate state.

## B. Shaped pulse with single-step phase patten of $\omega_{\text{step}}^{(\text{SNstep})} = \omega_{7p,4s}$

Next we consider the case of the shaped pulse with the phase pattern of a single  $\pi$  step at  $\omega_{\text{step}}^{(\text{SNstep})} = \omega_{7p,4s}$  (solid gray lines in Fig. 5). As the corresponding field  $\tilde{E}_{\text{SNstep}@\omega_{7p,4s}}(\omega_{7p,4s} + \delta)$  is a real positive or negative quantity for any  $\omega$ , the corresponding  $A_{\text{SNstep}@\omega_{7p,4s}}^{(2)}(\omega_{4s,3s} - \delta)$  is also a real quantity that, for a given spectrum, its positive or negative sign depends on  $\delta$ . This is seen in Fig. 5, where the difference from the TL case is clearly observable. Since the TL pulse induces fully constructive interferences among all the two-photon pathways that contribute to  $A^{(2)}(\Omega)$  for any given  $\Omega$ , with a given spectrum, the TL value of  $A_{\text{TL}}^{(2)}(\omega_{4s,3s} - \delta)$  is actually the maximal one for any given  $\delta$ . As such, it serves as an upper limit to the value of  $\left| A_{\text{SNstep}@\omega_{7p,4s}}^{(2)}(\omega_{4s,3s} - \delta) \right|$ .

As can be seen from Fig. 5, the values of  $A_{\text{SNstep}@\omega_{7p,4s}}^{(2)}(\omega_{4s,3s} - \delta)$  at  $\delta = 0$  and at  $\delta \approx 0$  strongly depend on the spectral bandwidth: with 5-nm and 9-nm bandwidth the values for  $\delta = 0$  and  $\delta \approx 0$  are all positive [panels (a) and (b)], with 15-nm bandwidth the value for  $\delta = 0$  is almost zero while the values for small  $\pm |\delta|$  are of different signs [panel (c)], and with 25-nm and 40-nm bandwidth the values for  $\delta = 0$  and  $\delta \approx 0$  are all negative [panels (d) and (e)]. On the other hand, with any spectral bandwidth, the field  $\tilde{E}_{\text{SNstep}@\omega_{7p,4s}}(\omega_{7p,4s} + \delta)$  has different sign for  $+\delta$  and  $-\delta$ , which is in full correlation with the corresponding sign of  $1/\delta$ . Thus, the relative sign between the amplitudes  $\frac{1}{\delta} A_{\text{SNstep}@\omega_{7p,4s}}^{(2+1)}(\delta)$  contributed by  $\pm |\delta|$  to the  $\wp$ -integration of  $A_{7p,\text{SNstep}@\omega_{7p,4s}}^{(2+1)\text{near-res}}$  is determined only by  $A_{\text{SNstep}@\omega_{7p,4s}}^{(2)}(\omega_{4s,3s} - \delta)$ . As such, it depends here on the spectral bandwidth. In Fig. 5, the  $A_{\text{SNstep}@\omega_{7p,4s}}^{(2)}(\omega_{4s,3s} - \delta)$  values for  $\pm |\delta|$  are of the same sign, i.e., they interfere constructively one with the other, in all the bandwidth cases except for the 15-nm bandwidth, where they are of different sign and thus interfere destructively one with the other. The constructive nature of these interferences generally leads to the dominance of the corresponding near-resonant component  $A_{7p,\text{SNstep}@\omega_{7p,4s}}^{(2+1)\text{near-res}}$  over the on-resonant component  $A_{7p,\text{SNstep}@\omega_{7p,4s}}^{(2+1)\text{on-res}}$  for all bandwidth values, except for values around 15 nm. There, both the near-resonant and on-resonant components are very small and have a value close to zero. This is indeed the behavior of the near-resonant vs. on-resonant components shown in Fig. 4(a).

For analyzing the bandwidth dependence of the absorption relative to the TL pulse, i.e., the graph of  $\tilde{P}_{7p,\text{SNstep}@\omega_{7p,4s}}^{(2+1)}$  vs.  $\Delta\omega$  shown in Fig. 4(a) (solid line), one also needs to account for the case of the TL pulse analyzed in the previous section. At a very narrow bandwidth

the phase shaping is expected to have very small or no effect at all on the absorption relative to the (unshaped) TL pulse, as is indeed reflected in the value  $\tilde{P}_{7p, \text{SNstep}@\omega_{7p,4s}}^{(2+1)} = 1$  for 2-nm bandwidth. Then, as the bandwidth increases the pulse shaping starts to have an effect. For the 5-nm bandwidth, where there is a local peak of  $\tilde{P}_{7p, \text{SNstep}@\omega_{7p,4s}}^{(2+1)} \sim 2.5$ , one obtains that: (i)  $\left| A_{7p, \text{SNstep}@\omega_{7p,4s}}^{(2+1)on-res} \right| \approx \left| A_{7p, \text{TL}}^{(2+1)on-res} \right|$  since  $A_{\text{SNstep}@\omega_{7p,4s}}^{(2)}(\omega_{4s,3s} - \delta) \approx A_{\text{TL}}^{(2)}(\omega_{4s,3s} - \delta)$  [see Fig. 5(a)], and (ii)  $\left| A_{7p, \text{SNstep}@\omega_{7p,4s}}^{(2+1)near-res} \right| > \left| A_{7p, \text{TL}}^{(2+1)near-res} \right|$  due to the different nature of the interferences between positively- and negatively-detuned excitation pathways for the two pulses. Hence,  $\tilde{P}_{7p, \text{SNstep}@\omega_{7p,4s}}^{(2+1)} = \frac{\left| A_{7p, \text{SNstep}@\omega_{7p,4s}}^{(2+1)on-res} \right|^2 + \left| A_{7p, \text{SNstep}@\omega_{7p,4s}}^{(2+1)near-res} \right|^2}{\left| A_{7p, \text{TL}}^{(2+1)on-res} \right|^2 + \left| A_{7p, \text{TL}}^{(2+1)near-res} \right|^2} > 1$  for 5-nm bandwidth. Then, as the bandwidth increases from 5 nm to 9 nm, the value of  $\tilde{P}_{7p, \text{SNstep}@\omega_{7p,4s}}^{(2+1)}$  decrease to a value around 1. This decrease results mainly from the stronger increase of  $A_{\text{TL}}^{(2)}(\omega_{4s,3s})$  relative to  $A_{\text{SNstep}@\omega_{7p,4s}}^{(2)}(\omega_{4s,3s} - \delta)$  for  $\delta = 0$  and  $\delta \approx 0$  [see Fig. 5(b)]. Then, as the bandwidth further increases to around 15 nm, the value of  $\tilde{P}_{7p, \text{SNstep}@\omega_{7p,4s}}^{(2+1)}$  approach zero since  $\left| A_{7p, \text{SNstep}@\omega_{7p,4s}}^{(2+1)on-res} \right| \approx 0$  and  $\left| A_{7p, \text{SNstep}@\omega_{7p,4s}}^{(2+1)near-res} \right| \approx 0$ , resulting from  $A_{\text{SNstep}@\omega_{7p,4s}}^{(2)}(\omega_{4s,3s}) \approx 0$  and  $A_{\text{SNstep}@\omega_{7p,4s}}^{(2)}(\omega_{4s,3s} - \delta) \approx 0$  for  $\delta \approx 0$  [see above and Fig. 5(c)]. Actually, with 14.6-nm bandwidth the on-resonant component is completely zeroing out and to a very good approximation the corresponding shaped pulse is a three-photon dark pulse.

Further increase of the bandwidth beyond 15 nm, leads to a continuous increase in the value of  $\tilde{P}_{7p, \text{SNstep}@\omega_{7p,4s}}^{(2+1)}$ . For example, at 40-nm bandwidth it reaches a value of 4.1. Following the above analysis and as seen in Fig. 3(d1)-(e1) and Fig. 4(a), for bandwidth values beyond 15 nm, the value of  $\tilde{P}_{7p, \text{SNstep}@\omega_{7p,4s}}^{(2+1)}$  is actually determined only by the dominant near-resonant shaped-pulse term  $\left| A_{7p, \text{SNstep}@\omega_{7p,4s}}^{(2+1)near-res} \right|$  and the on-resonant TL term  $\left| A_{7p, \text{TL}}^{(2+1)on-res} \right|$ , i.e.,  $\tilde{P}_{7p, \text{SNstep}@\omega_{7p,4s}}^{(2+1)} \approx \left| A_{7p, \text{SNstep}@\omega_{7p,4s}}^{(2+1)near-res} \right|^2 / \left| A_{7p, \text{TL}}^{(2+1)on-res} \right|^2$ . For large bandwidth  $\Delta\omega$ ,  $\tilde{E}(\omega_{7p,4s}) \approx \tilde{E}(\omega_0) \equiv 1$  and  $\tilde{E}(\omega_{7p,4s} - \delta) \approx \tilde{E}(\omega_0) \equiv 1$  for small  $\delta$ . Hence: (i) For the TL pulse: since  $A_{\text{TL}}^{(2)}(\omega_{4s,3s}) \propto \Delta\omega$ , based on Eq. (3),  $\left| A_{7p, \text{TL}}^{(2+1)on-res} \right| = k_1 \Delta\omega$ , where  $k_1$  is a proportionality constant for the TL pulse; (ii) For the shaped pulse of  $\omega_{\text{step}}^{(\text{SNstep})} = \omega_{7p,4s}$ :  $A_{7p, \text{SNstep}@\omega_{7p,4s}}^{(2+1)near-res} = -\wp \int_{-\infty}^{\infty} \frac{1}{\delta} A^{(2)}(\omega_{4s,3s} - \delta) d\delta = k_{2a} \Delta\omega + k_{2b} \Delta\omega \ln \Delta\omega$ , where  $k_{2a}$  and  $k_{2b}$  are constants for the specific single-step pulse shape. As a result, for large enough bandwidth values, an increase in the bandwidth  $\Delta\omega$  leads to a continuous increase in the value of  $\tilde{P}_{7p, \text{SNstep}@\omega_{7p,4s}}^{(2+1)}$  as  $K_{2a} + K_{2b} \ln \Delta\omega$ . This is indeed seen in the graph shown in Fig. 4(a) (solid line).

### C. Shaped pulse with double-step phase pattern of $\omega_{\text{left-step}}^{(\text{DBstep})} = \omega_{7p,4s}$

Last we consider the case of the shaped pulse with the phase pattern of a double  $\pi$  step with  $\omega_{\text{left-step}}^{(\text{DBstep})} = \omega_{7p,4s}$  (solid thin black lines in Fig. 5). With such a phase pattern, as with any of the double-step phase patterns, the phase associated with all the two-photon pathways of total two-photon transition frequency  $\omega_{4s,3s}$  is zero, since  $\Phi(\omega) + \Phi(\omega_{4s,3s} - \omega) = 0$  for any  $\omega$  (see Fig. 1). So, fully constructive interferences are induced between all these two-photon pathways, as is the case with the transform-limited pulse. Hence, as seen in Fig. 5, with any spectral bandwidth,  $A_{\text{DBstep}@\omega_{7p,4s}}^{(2)}(\omega_{4s,3s}) = A_{\text{TL}}^{(2)}(\omega_{4s,3s})$ , which, as explained above, is the maximal possible value (here, at  $\delta = 0$ ) for a given spectrum. This leads to a maximal on-resonant amplitude that is of equal magnitude to the TL case, i.e.,  $\left| A_{7p,\text{DBstep}@\omega_{7p,4s}}^{(2+1)\text{on-res}} \right| = \left| A_{7p,\text{TL}}^{(2+1)\text{on-res}} \right|$ , for any bandwidth  $\Delta\omega$ .

With the double-step phase pattern of  $\omega_{\text{left-step}}^{(\text{DBstep})} = \omega_{7p,4s}$ , the field  $\tilde{E}_{\text{DBstep}@\omega_{7p,4s}}(\omega_{7p,4s} + \delta)$  has different sign for  $\pm|\delta|$  when  $|\delta|$  is small, which is in full correlation with the sign of  $1/\delta$  for small  $\pm|\delta|$ . This is similar to the case of the single-step phase pattern of  $\omega_{\text{step}}^{(\text{SNstep})} = \omega_{7p,4s}$  discussed above. Thus, also here, the relative sign between the amplitudes  $\frac{1}{\delta} A_{\text{DBstep}@\omega_{7p,4s}}^{(2+1)}(\delta)$  contributed to the  $\wp$ -integration of  $A_{7p,\text{DBstep}@\omega_{7p,4s}}^{(2+1)\text{near-res}}$  from  $\pm|\delta|$  is determined only by  $A_{\text{DBstep}@\omega_{7p,4s}}^{(2)}(\omega_{4s,3s} - \delta)$ .

The fact that  $A_{\text{DBstep}@\omega_{7p,4s}}^{(2)}(\omega_{4s,3s})$  (i.e., for  $\delta = 0$ ) has the maximal possible value also implies that for small  $\delta$  values  $A_{\text{DBstep}@\omega_{7p,4s}}^{(2)}(\omega_{4s,3s} - \delta)$  is also very close to the maximal possible TL value, i.e.,  $A_{\text{DBstep}@\omega_{7p,4s}}^{(2)}(\omega_{4s,3s} - \delta) \approx A_{\text{TL}}^{(2)}(\omega_{4s,3s} - \delta)$ , with a corresponding value that is a real positive one. As seen in Fig. 5, for any bandwidth,  $A_{\text{DBstep}@\omega_{7p,4s}}^{(2)}(\omega_{4s,3s} - \delta)$  is of the same sign for small  $\pm|\delta|$ , i.e., the interferences between negatively- and positively-detuned near-resonant pathways are constructive ones. Similar to the single-step phase pattern discussed above, the constructive nature of these interferences leads to the dominance of the corresponding near-resonant component  $A_{7p,\text{DBstep}@\omega_{7p,4s}}^{(2+1)\text{near-res}}$  over the on-resonant component  $A_{7p,\text{DBstep}@\omega_{7p,4s}}^{(2+1)\text{on-res}}$  for all bandwidth values. This is indeed the behavior of the near-resonant vs. on-resonant components shown in Fig. 4(b). The fact that  $A_{\text{DBstep}@\omega_{7p,4s}}^{(2)}(\omega_{4s,3s} - \delta) \approx A_{\text{TL}}^{(2)}(\omega_{4s,3s} - \delta)$ , while the nature of the near-resonant interferences is constructive to the pulse with the double-step phase pattern and destructive for the TL pulse, imply that  $\left| A_{7p,\text{DBstep}@\omega_{7p,4s}}^{(2+1)\text{near-res}} \right|^2 \gg \left| A_{7p,\text{TL}}^{(2+1)\text{near-res}} \right|^2$ .

The overall bandwidth dependence of  $\tilde{P}_{7p,\text{DBstep}@\omega_{7p,4s}}^{(2+1)}$  shown in Fig. 4(b) (solid line),

can then be understood as follows: Since  $\left|A_{7p,\text{DBstep}@}\omega_{7p,4s}^{(2+1)\text{on-res}}\right|^2 = \left|A_{7p,\text{TL}}^{(2+1)\text{on-res}}\right|^2$  and  $\left|A_{7p,\text{DBstep}@}\omega_{7p,4s}^{(2+1)\text{near-res}}\right|^2 > \left|A_{7p,\text{TL}}^{(2+1)\text{near-res}}\right|^2$  one obtains that  $\tilde{P}_{7p,\text{DBstep}@}\omega_{7p,4s}^{(2+1)} > 1$  for any bandwidth value. This is indeed what observed in Fig. 4(b), i.e., the corresponding three-photon absorption is always above the TL absorption.

The asymptotic behavior of the graph of  $\tilde{P}_{7p,\text{DBstep}@}\omega_{7p,4s}^{(2+1)}$ -vs.- $\Delta\omega$  is actually very similar to the single-step phase pattern case analyzed above, just with higher values due to the fact that  $A_{\text{DBstep}@}\omega_{7p,4s}^{(2)}(\omega_{4s,3s})$  is kept on its maximal value for any bandwidth. Also here, for large bandwidth  $\Delta\omega$ , following the above analysis for the present double-phase-step pulse and for the TL pulse,  $\tilde{P}_{7p,\text{DBstep}@}\omega_{7p,4s}^{(2+1)} \approx \left|A_{7p,\text{DBstep}@}\omega_{7p,4s}^{(2+1)\text{near-res}}\right|^2 / \left|A_{7p,\text{TL}}^{(2+1)\text{on-res}}\right|^2$ . Also,  $\tilde{E}(\omega_{7p,4s}) \approx \tilde{E}(\omega_0) \equiv 1$  and  $\tilde{E}(\omega_{7p,4s} - \delta) \approx \tilde{E}(\omega_0) \equiv 1$  for small  $\delta$ . So: (i) For the TL pulse:  $A_{\text{TL}}^{(2)}(\omega_{4s,3s}) \propto \Delta\omega$  and thus  $\left|A_{7p,\text{TL}}^{(2+1)\text{on-res}}\right| = k_1\Delta\omega$ , where  $k_1$  is the TL proportionality constant. (ii) For the shaped pulse of  $\omega_{\text{left-step}}^{(\text{DBstep})} = \omega_{7p,4s}$ :  $A_{7p,\text{DBstep}@}\omega_{7p,4s}^{(2+1)\text{near-res}} = -\wp \int_{-\infty}^{\infty} \frac{1}{\delta} A^{(2)}(\omega_{4s,3s} - \delta) d\delta = k_{3a}\Delta\omega + k_{3b}\Delta\omega \ln \Delta\omega$ , where  $k_{3a}$  and  $k_{3b}$  are constants for the specific double-phase-step pulse shape. So,  $\tilde{P}_{7p,\text{DBstep}@}\omega_{7p,4s}^{(2+1)}$  behaves asymptotically as  $K_{3a} + K_{3b} \ln \Delta\omega$ . The constants  $K_{3a}$  and  $K_{3b}$  are, respectively, larger than the  $K_{2a}$  and  $K_{2b}$  constants of the single-step phase pattern of  $\omega_{\text{step}}^{(\text{SNstep})} = \omega_{7p,4s}$ , due to the larger near-resonant component induced by the double-step phase pattern. Hence, for any given bandwidth, the resonance-mediated (2+1) three-photon absorption induced by the shaped pulse with double-step phase pattern of  $\omega_{\text{left-step}}^{(\text{DBstep})} = \omega_{7p,4s}$  is higher than the absorption induced by the shaped pulse with single-step phase pattern of  $\omega_{\text{step}}^{(\text{SNstep})} = \omega_{7p,4s}$ .

## V. CONCLUSIONS

In conclusion, we have studied in detail femtosecond phase control of atomic resonance-mediated (2+1) three-photon absorption, focusing on its dependence on the spectral bandwidth of the excitation pulse. The total absorption amplitude has contributions from a group of interfering three-photon pathways that are on resonant with the intermediate state and a group of interfering three-photon pathways that are near resonant with it. For a given pulse shape, the ratio between the amplitude contributions from these two groups depends on the spectral excitation bandwidth. The nature of the three-photon absorption that is induced by a given shaped pulse is analyzed in a systematic and physically-intuitive way by decomposing it into a two-photon absorption, which is induced by all the possible two-

photon pathways leading to various detunings from the intermediate state, followed by the absorption of a proper third photon. Prominent among the results is our finding that with simple proper pulse shaping an increase in the excitation bandwidth leads to a corresponding increase in the enhancement of the three-photon absorption over the absorption induced by the (unshaped) transform-limited pulse. For example, here, 40-nm bandwidth leads to an order-of-magnitude enhancement over the transform-limited absorption. The present work serves as a basis for future extensions to molecular systems and we expect it to be significant for nonlinear spectroscopy and microscopy.

### **ACKNOWLEDGMENTS**

This research was supported by The Israel Science Foundation (grant No. 127/02), by The James Franck Program in Laser Matter Interaction, and by The Technion's Fund for The Promotion of Research.



- 
- [1] D. J. Tannor, R. Kosloff, and S. A. Rice, *J. Chem. Phys.* **85**, 5805 (1986).
- [2] M. Shapiro and P. Brumer, *Principles of the quantum control of molecular processes* (Wiley, New Jersey, 2003).
- [3] W. S. Warren, H. Rabitz, and D. Mahleh, *Science* **259**, 1581 (1993).
- [4] H. Rabitz, R. de Vivie-Riedle, M. Motzkus, and K. Kompa, *Science* **288**, 824 (2000).
- [5] M. Dantus and V. V. Lozovoy, *Chem. Rev.* **104**, 1813 (2004); *ChemPhysChem* **6**, 1970 (2005).
- [6] D. Meshulach and Y. Silberberg, *Nature (London)* **396**, 239 (1998); *Phys. Rev. A* **60**, 1287 (1999).
- [7] A. Präkelt *et al.*, *Phys. Rev. A* **70**, 063407 (2004).
- [8] N. Dudovich *et al.*, *Phys. Rev. Lett.* **86**, 47 (2001).
- [9] B. Chatel, J. Degert, and B. Girard, *Phys. Rev. A* **70**, 053414 (2004).
- [10] P. Panek and A. Becker, *Phys. Rev. A* **74**, 023408 (2006).
- [11] K. A. Walowicz *et al.*, *J. Phys. Chem. A* **106**, 9369 (2002); V. V. Lozovoy *et al.*, *J. Chem. Phys.* **118**, 3187 (2003).
- [12] H. U. Stauffer *et al.*, *J. Chem. Phys.* **116**, 946 (2002); X. Dai, E. W. Lerch, and S. R. Leone, *Phys. Rev. A* **73**, 023404 (2006).
- [13] D. Oron *et al.*, *Phys. Rev. A* **65**, 043408 (2002); N. Dudovich, D. Oron, and Y. Silberberg, *Nature (London)* **418**, 512 (2002);
- [14] S. Lim, A. G. Caster, and S. R. Leone, *Phys. Rev. A* **72**, 041803 (2005);
- [15] A. Gandman, L. Chuntunov, L. Rybak, and Z. Amitay, *Phys. Rev. A* **75**, 031401 (R) (2007).
- [16] E. Gershgoren *et al.*, *Opt. Lett.* **28**, 361 (2003).
- [17] B. Yellampalle *et al.*, *Opt. Exp.* **13**, 7672 (2005).
- [18] L. Chuntunov, L. Rybak, A. Gandman, and Z. Amitay, submitted for publication.
- [19] N. Dudovich *et al.*, *Phys. Rev. Lett.* **94**, 083002 (2005).
- [20] C. Trallero-Herrero *et al.*, *Phys. Rev. A* **71**, 013423 (2005); *Phys. Rev. Lett.* **96**, 063603 (2006).
- [21] M. Wollenhaupt *et al.*, *Phys. Rev. A* **68**, 015401 (2003); *Phys. Rev. A* **73**, 063409 (2006);
- [22] A. M. Weiner, *Rev. Sci. Inst.* **71**, 1929 (2000).
- [23] NIST Atomic Spectra Database (National Institute of Standards and Technology, Gaithers-

burg, MD), available at <http://physics.nist.gov/asd>

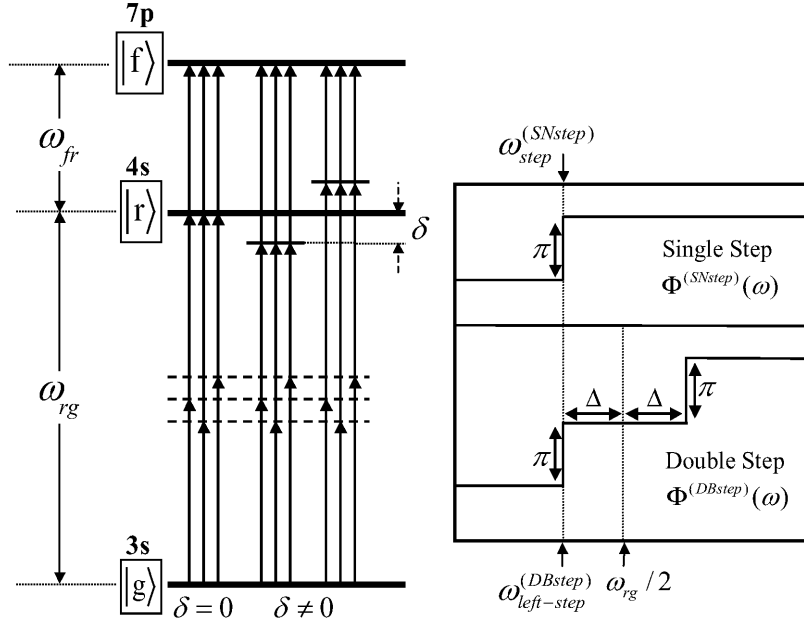


FIG. 1: The resonance-mediated (2+1) three-photon excitation scheme (not to scale) from  $|g\rangle$  to  $|f\rangle$  via  $|r\rangle$ . The corresponding Na states are, respectively,  $3s$ ,  $4s$ , and  $7p$ . Several sets of pathways that are on resonance ( $\delta = 0$ ) and near resonance ( $\delta \neq 0$ ) with  $|r\rangle \equiv 4s$  are shown;  $\delta$  is the corresponding detuning. Also shown schematically are examples of the two types of spectral phase patterns used in the study,  $\Phi^{(SNstep)}(\omega)$  and  $\Phi^{(DBstep)}(\omega)$ . The  $\Phi^{(SNstep)}(\omega)$  set includes the phase patterns with a single  $\pi$  step, each is characterized by the  $\pi$  step position  $\omega_{step}^{(SNstep)}$ . The  $\Phi^{(DBstep)}(\omega)$  set includes the phase patterns composed of two  $\pi$  steps, with the two steps located at equal distance along the frequency axis from both sides of half the two-photon transition frequency  $\omega_{rg}/2$ . Each such double-step pattern is characterized by the position of the left step  $\omega_{left-step}^{(DBstep)}$ .

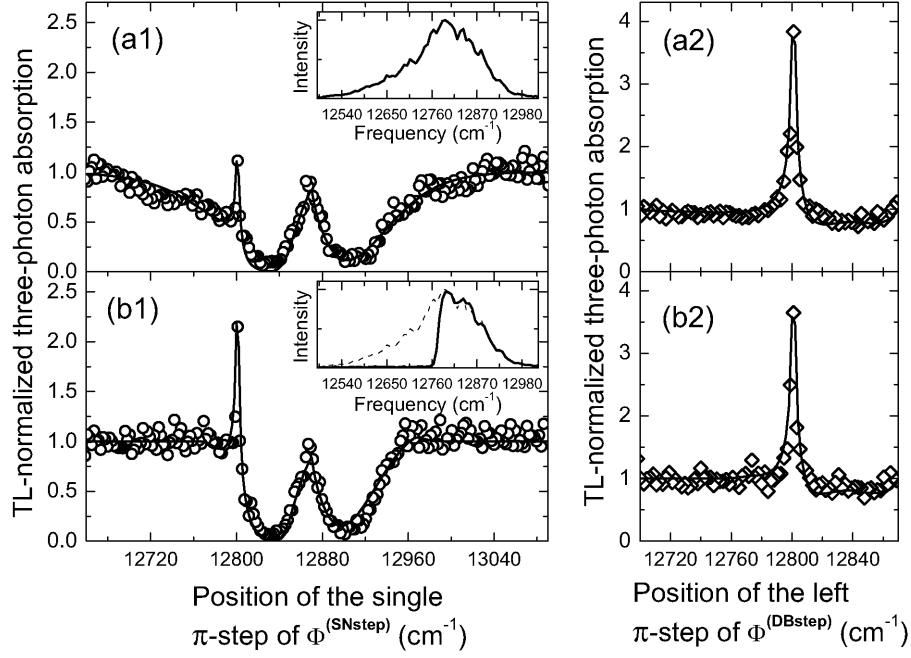


FIG. 2: Experimental (circles and squares) and numerical-theoretical (solid lines) results for the resonance-mediated (2+1) three-photon absorption in Na. Panels (a1) and (a2) correspond to the full pulse spectrum [inset of (a1)], while panels (b1) and (b2) correspond to the blocked pulse spectrum [inset of (b1)]. Panels (a1) and (b1) (left-column panels) present results for the single-step set of spectral phase patterns  $\Phi^{(\text{SNstep})}(\omega)$ . The corresponding traces show the TL-normalized final  $7p$  population  $\tilde{P}_{7p}^{(2+1)}$  (see text) as a function of the single  $\pi$ -step position  $\omega_{\text{step}}^{(\text{SNstep})}$ . Panels (a2) and (b2) (right-column panels) present results for the double-step set of spectral phase patterns  $\Phi^{(\text{DBstep})}(\omega)$ . The corresponding traces show the TL-normalized final  $7p$  population  $\tilde{P}_{7p}^{(2+1)}$  (see text) as a function of the left  $\pi$ -step position  $\omega_{\text{left-step}}^{(\text{DBstep})}$ .

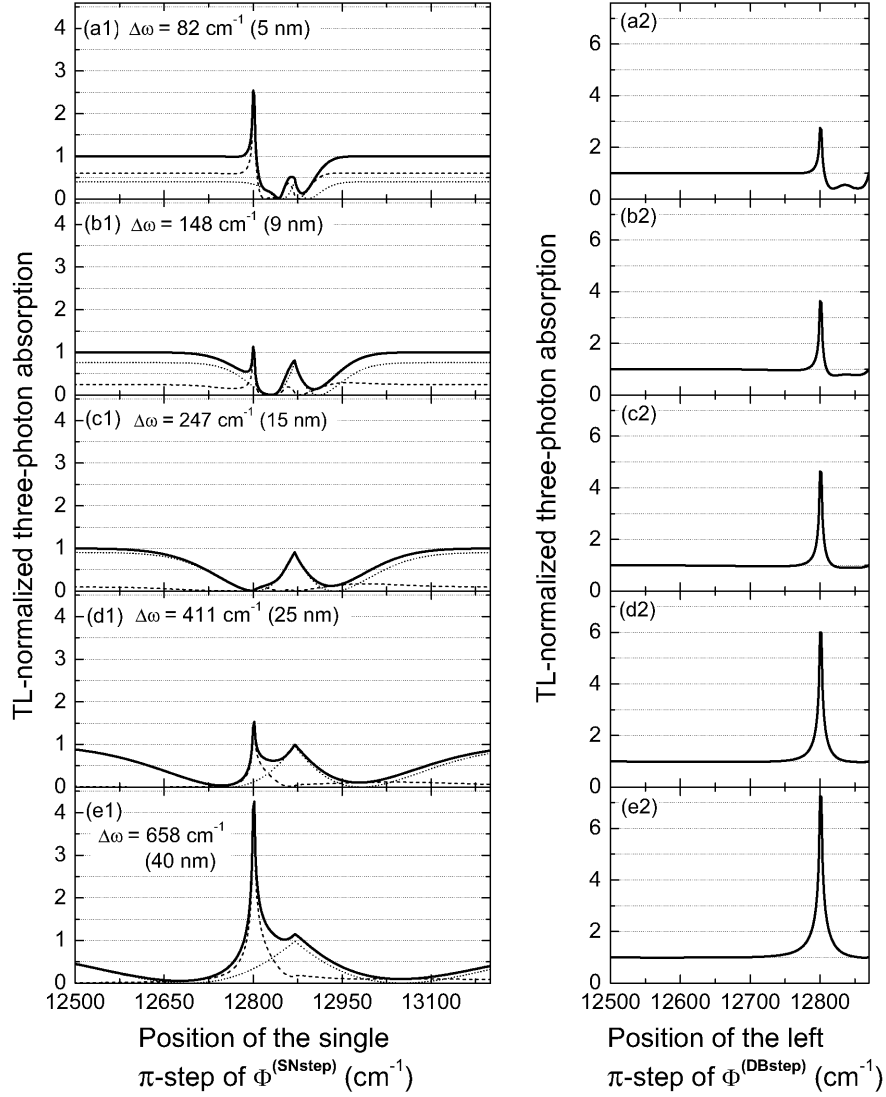


FIG. 3: Theoretical results (solid lines) of the resonance-mediated (2+1) three-photon absorption in Na calculated with excitation pulse of different spectral intensity bandwidth  $\Delta\omega$ . In all the cases the pulse spectrum is a Gaussian centered at 780 nm ( $12821 \text{ cm}^{-1}$ ). Each row in the figure corresponds to a different bandwidth. The left-column panels correspond to the single-step spectral phase patterns  $\Phi^{(\text{SNstep})}(\omega)$ . They show the TL-normalized final  $7p$  population  $\tilde{P}_{7p}^{(2+1)}$  (solid lines) as a function of the single  $\pi$ -step position  $\omega_{\text{step}}^{(\text{SNstep})}$ . Additionally, they also show the corresponding on-resonant component  $|\tilde{A}_{7p}^{(2+1)\text{on-res}}|^2$  (dotted lines) and near-resonant component  $|\tilde{A}_{7p}^{(2+1)\text{near-res}}|^2$  (dashed lines). The right-column panels correspond to the double-step spectral phase patterns  $\Phi^{(\text{DBstep})}(\omega)$ . They show the TL-normalized final  $7p$  population  $\tilde{P}_{7p}^{(2+1)}$  as a function of the left  $\pi$ -step position  $\omega_{\text{left-step}}^{(\text{DBstep})}$ .

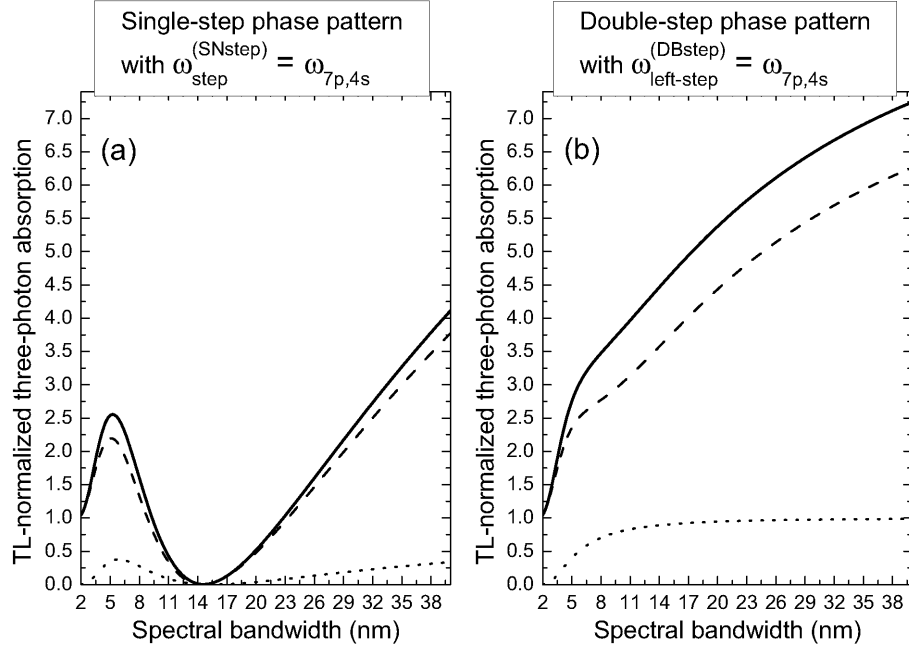


FIG. 4: Numerical-theoretical results for the dependence of the resonance-mediated (2+1) three-photon absorption in Na on the spectral intensity bandwidth of the excitation pulse having (a) single-step phase pattern of  $\omega_{\text{step}}^{(\text{SNstep})} = \omega_{7p,4s}$ , and (b) double-step phase pattern of  $\omega_{\text{left-step}}^{(\text{DBstep})} = \omega_{7p,4s}$ . Shown are  $\tilde{P}_f^{(2+1)}$  (solid lines),  $|\tilde{A}_{7p}^{(2+1)\text{on-res}}|^2$  (dotted lines), and  $|\tilde{A}_{7p}^{(2+1)\text{near-res}}|^2$  (dashed lines) as a function of the spectral bandwidth  $\Delta\omega$ .

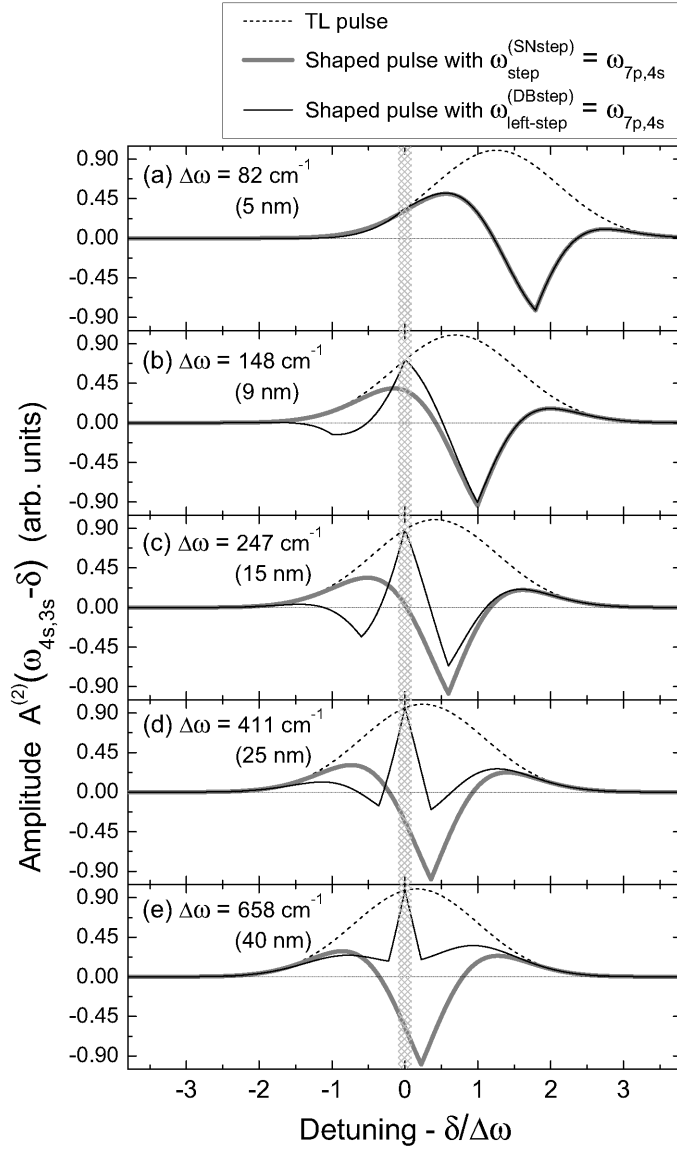


FIG. 5: Numerical-theoretical results for the values of  $A^{(2)}(\Omega = \omega_{4s,3s} - \delta)$  [see Eq. (5)] as a function of the detuning  $\delta$  for different spectral intensity bandwidth  $\Delta\omega$  of the excitation pulse. In all the cases the pulse spectrum is a Gaussian centered at 780 nm ( $12821 \text{ cm}^{-1}$ ). The different panels correspond to the different panels in Fig. 3. The detuning values are given as normalized values  $\delta/\Delta\omega$  (see text). Each panel shows results for the transform-limited (TL) pulse (dashed black line), for the shaped pulse with the single-step phase pattern of  $\omega_{\text{step}}^{(\text{SNstep})} = \omega_{7p,4s}$  (solid gray line), and for the shaped pulse with the double-step phase pattern of  $\omega_{\text{left-step}}^{(\text{DBstep})} = \omega_{7p,4s}$  (solid black line).